

# Nanoscale

Accepted Manuscript



This is an *Accepted Manuscript*, which has been through the Royal Society of Chemistry peer review process and has been accepted for publication.

*Accepted Manuscripts* are published online shortly after acceptance, before technical editing, formatting and proof reading. Using this free service, authors can make their results available to the community, in citable form, before we publish the edited article. We will replace this *Accepted Manuscript* with the edited and formatted *Advance Article* as soon as it is available.

You can find more information about *Accepted Manuscripts* in the [Information for Authors](#).

Please note that technical editing may introduce minor changes to the text and/or graphics, which may alter content. The journal's standard [Terms & Conditions](#) and the [Ethical guidelines](#) still apply. In no event shall the Royal Society of Chemistry be held responsible for any errors or omissions in this *Accepted Manuscript* or any consequences arising from the use of any information it contains.

Cite this: DOI: 10.1039/c0xx00000x

www.rsc.org/xxxxxx

ARTICLE TYPE

# Polysaccharide Nano-vesicular Multidrug Carrier for Synergistic Killing of Cancer Cells

P.S. Pramod<sup>a†</sup>, Ruchira Shah<sup>b‡</sup>, Sonali Chaphekar<sup>b</sup>, Nagaraj Balasubramanian<sup>b\*</sup>, and Manickam Jayakannan<sup>a\*</sup>

Received (in XXX, XXX) Xth XXXXXXXXXX 20XX, Accepted Xth XXXXXXXXXX 20XX

DOI: 10.1039/b000000x

Multi-drug delivery based on polymer nano-scaffolds is an essential protocol to be developed for better administration of anticancer drugs to enhance their therapeutic efficacies against cancer cells. Here, we report dual delivery polysaccharide nano-vesicles that are capable of loading and delivering both water soluble and water insoluble drugs together in a single polymer scaffold. The selective rupture of the nano-vesicular assembly by intracellular enzyme conditions allowed the simultaneous delivery of hydrophobic drug camptothecin (CPT) and hydrophilic drug doxorubicin (DOX) supporting their synergistic killing of breast and colon cancer cells. The polysaccharide nano-vesicles have allowed us to address a few important questions regarding the need for multiple drug administration in cancer cells including a) the role of simultaneous drug release, b) antagonistic versus synergistic effects of drug combinations and c) how these are affected by the ratio of drugs. Further, evaluation of the role of caveolae in endocytosis of these polymer scaffolds was also made. The vesicular scaffolds were found to preserve and deliver DOX resulting in 50–60% better killing of cancer cells than the free drug. Additionally, dual loaded nano-vesicles when compared to drug cocktails with individual drugs in separate nano-vesicles (at comparable molar ratios) suggest the relative drug concentration following release and mode of delivery to be both important in cancer cell killing. Results from these experiments have revealed that newly developed polysaccharide nano-vesicles loaded with DOX and CPT drugs as potential candidates for improved breast cancer cell killing. Thus, these custom-designed polysaccharide nano-vesicles provide a new perspective on multi-anticancer drug delivery systems and their efficacy.

## 1 Introduction

Multi-drug delivery from single nano-carrier is an important approach for the administration of anticancer drugs to overcome tumor resistance to individual drugs and enhance their therapeutic efficacies.<sup>1–4</sup> Polymer vesicles (or polymersomes) are unique nano-carriers for the above purpose due to their ability to load and deliver the combination of hydrophilic and hydrophobic drugs in the core and layer, respectively.<sup>5–7</sup> These synthetic vesicles inherently possess advantages such as tunable size and shapes, stimuli-response delivery, higher drug loading capacity and longer blood circulation time when compared to other nano-carriers such as liposomes and micelles.<sup>8–11</sup> Amphiphilic block copolymers<sup>12–15</sup>, random and graft copolymers<sup>16</sup>, polysaccharide derivatives<sup>17–19</sup>, dendrimers<sup>20,21</sup> and hyperbranched polymers<sup>22–24</sup> are some of the candidates used for making polymeric vesicles. In last 3 years, a few attempts were made to employ polymer vesicles for combination therapy of multiple anticancer drugs based on blends of PEGlated polybutadiene/polylactide<sup>25</sup>, lipid coated poly(lactide)s,<sup>26</sup> and Glutathione (GSH) responsive triblocks<sup>27</sup>. These preliminary studies highlight the potential of polymer vesicular assemblies that are only now being explored for clinical applications<sup>28</sup>. The success of a polymer vesicular

scaffold (or any other nano-carriers) for multi-drug delivery is dependent on several parameters including the ability of the polymer vesicle to load more than one drug under identical conditions, its ability to preserve their pharmacophore and its ability to release these drugs in a controlled manner. Their action could further be supported by an understanding of the target cells selectivity for the uptake of the polymer scaffolds and the cells ability to release the drug from the vesicle following their uptake. Though, polysaccharide nano-scaffolds are widely studied for anticancer drug delivery;<sup>29</sup> their cellular uptake mechanism with respect to the type of cancer cells and the administration of multidrug delivery based on polysaccharide is not understood.

Typically, self-organized polymeric structures choose either endocytic (caveolae, clathrin), phagocytic or pinocytic pathways for cellular internalization.<sup>30,31</sup> Depending on the kind of polymeric structures and the cell type the relative role of these different uptake mechanisms could vary (see figure 1a and 1b). Caveolin-1 for example is also a known tumor suppressor whose levels are down regulated in many cancers causing a loss of caveolae and affecting the cells endocytic uptake potential.<sup>32</sup> A careful and complete evaluation of the role of caveolar and other uptake pathways in polymer or nano-drug carrier delivery, particularly in context of specific cancers, remains to be made.

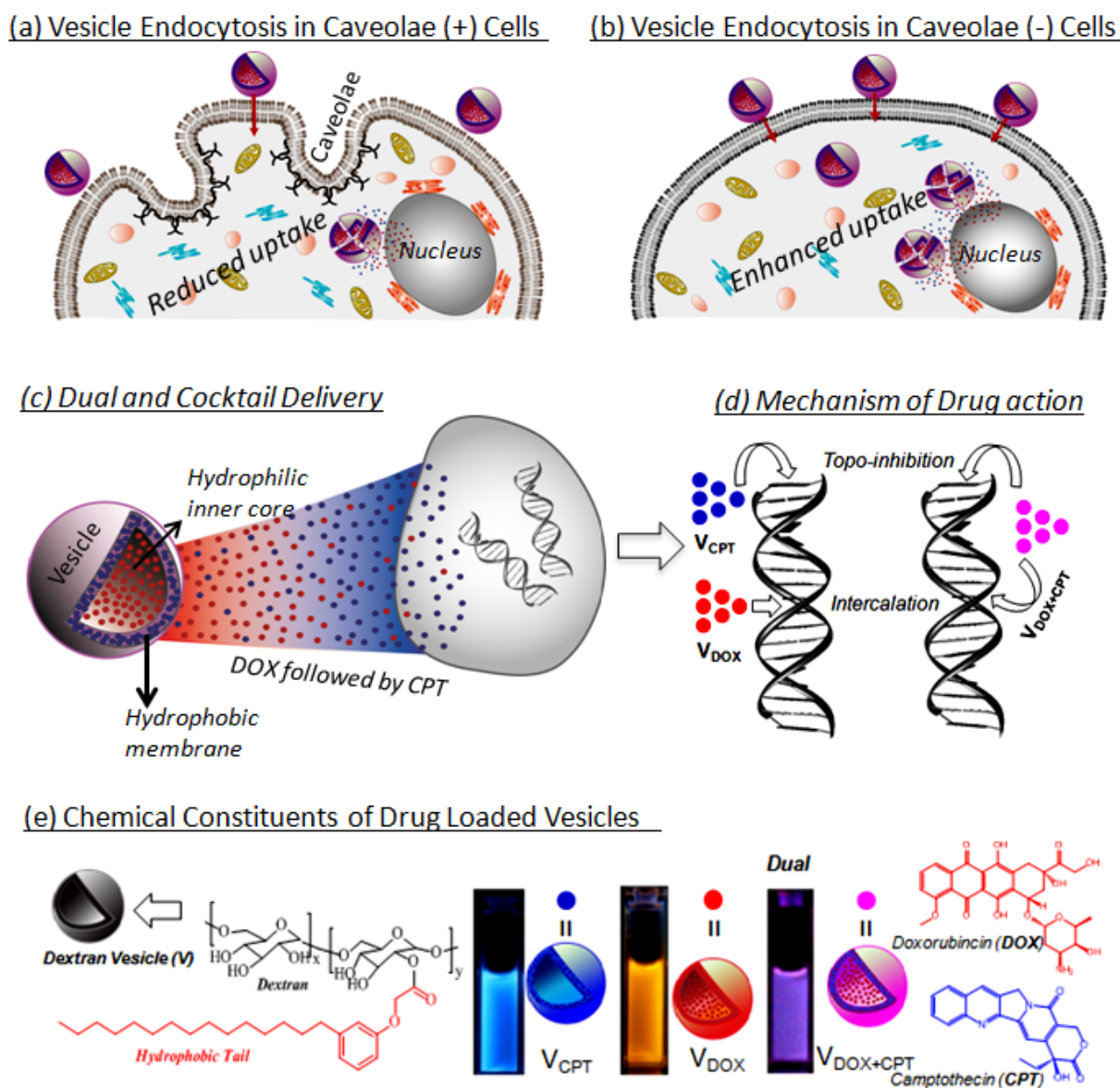


**Fig.1** Endocytosis of vesicles in caveolae containing cell (a), caveolae lacking cancer cell (b). (c) Schematic representation of mechanism of dual drug loaded and individual cocktails of vesicle. (d) Mechanism of action of DOX loaded, CPT loaded and dual drug loaded nano-vesicles. (e) Chemical structure of hydrophobically modified dextran, vesicle solution of CPT loaded ( $V_{CPT}$ ), DOX loaded ( $V_{DOX}$ ), dual drug loaded ( $V_{DOX+CPT}$ ) and Chemical structure of DOX and CPT. The colors of the vesicles represent their luminescent features under photoexcitation

Further, the choice of drugs for administration in combination could be dependent among other things on their mode of action and their chemical properties. Earlier studies have suggested that a combination of topoisomerases I (eg. CPT) and topoisomerases II (eg. DOX) inhibitors may be synergistic when administered together<sup>33</sup> as is the administration of histone deacetylase inhibitors (HDACi) and topoisomerases II (DOX)<sup>34</sup>. Simultaneous administration of these drugs in cancer cells was shown by Pavillard et al. to reveal that the administration of CPT followed by DOX showed synergistic killing effect, whereas the reverse caused antagonism.<sup>35</sup> Moreover, the concentrations and compositions of the drugs were also found to play a major role in the killing of cancer cells. Drug combinations could also run into this problem of differential solubility that could affect their

20 efficient delivery, eg CPT - hydrophobic and water insoluble and DOX.HCl - hydrophilic and water-soluble. Loading two such anticancer drugs (eg CPT and DOX) and achieving their simultaneous or sequential delivery (CPT followed by DOX) (see figure 1c) in a single polymer carrier could provide a major advantage in targeting cancers (see figure 1d).<sup>36</sup> Recently from our group, we reported a new renewable resource modified polysaccharide (dextran) based nano-vesicles for loading and delivering the CPT. The dextran scaffold was found to show two fold better killing of mouse fibroblast cells compared to free drug.<sup>37,38</sup> However, the ability of this scaffold to hold and deliver a hydrophilic and hydrophobic anticancer drug combination (like CPT and DOX.HCl) together in the single polysaccharide vesicular scaffold and their mechanism of cellular uptake of

cancer cells remained to be tested.

The present work aims to test the loading and administering of water soluble anticancer drug DOX (topoisomerases II inhibitor)<sup>39</sup> and water insoluble drug CPT (topoisomerases I inhibitor) in a single polymer polysaccharide nano-vesicles looking at their synergistic ability in killing of cancer cells (see Figure 1). This polysaccharide nano-vesicle developed earlier (see figure 1) constitutes a hydrophilic dextran backbone attached with hydrophobic renewable resource pentadecyl phenol (PDP) through an enzyme cleavable aliphatic ester linkage<sup>37</sup>. Under intracellular conditions; thus, the dextran nano-vesicular scaffold could rupture in the presence of the esterase enzyme (available in the lysosomal compartment) to deliver the loaded drugs (see figure 1e). This nano-vesicle design allows us to investigate the following questions associated with multiple drugs administration: (i) the synergistic / antagonistic role of these drugs in normal vs cancer cells, (ii) the role of drug ratios (ratiometric effect) in mediating cell killing in normal vs cancer cells, (iii) the effectiveness of dual drug loaded single-vesicle versus the cocktail of individual drug loaded nano-vesicles. The results provide significant new insights into polysaccharide loaded dual drug action of DOX:CPT drug combination in the breast and colon cancer cells.

## 2 Experimental Section:

**2.1 Materials:** Dextran ( $M_w = 6,000$ ), 3-pentadecylphenol, dicyclohexylcarbodiimide, 4-dimethylamino pyridine, pyrene, 20-(S)-camptothecin (CPT) and horse liver esterase enzyme were purchased from Aldrich chemicals. Dimethyl sulphoxide was dried over  $\text{CaH}_2$  and distilled prior to use. Ethyl chloroacetate,  $\text{K}_2\text{CO}_3$ , KI, KOH, and all other reagents and solvents were purchased locally and purified following the standard procedure. Wild type mouse embryonic fibroblasts (WT-MEFs), Caveolin1 knock out MEFs (Cav1<sup>-/-</sup>-MEFs) and Human breast cancer cells (MCF7) were maintained in DMEM (phenol red free medium: Gibco) containing 10% (v/v) fetal bovine serum (FBS) and 1% (v/v) penicillin-streptomycin at 37° C under a 5%  $\text{CO}_2$  humidified atmosphere. Under similar conditions, RPMI 1640, medium was used for colon cancer (DLD1) cell lines. Cells were washed with DPBS (Gibco), trypsinised using 0.05% trypsin (Gibco) and seeded in 96 well or 6 well (as per experiment) flat bottomed plastic plates (Costar) for all assays. Tetrazolium salt, 3-4,5 dimethylthiazol-2,5-diphenyltetrazolium bromide (MTT), DMSO, DAPI, Fibronectin (human Plasma) and paraformaldehyde was obtained from Sigma. Phalloidin conjugated to Alexa 488 was obtained from Molecular Probes (Invitrogen) and fluoromount from Southern Biotech. Antibodies: Monoclonal anti- $\beta$ -tubulin antibody (E7) was from Developmental Studies Hybridoma Bank (Iowa City, IA) and Anti-Caveolin antibody was from Santa Cruz Biotechnology (Cat# sc894)(Santa Cruz,CA). Goat anti-mouse HRP (Cat#115-035-003) and affinity purified Goat anti-rabbit HRP (Cat#111-035-003) were from Jacksons Immuno Research Labs,INC. Lysis Buffer: contains 1M Tris-Cl (pH-6.8) (Affymetrix, Cat#75825), 2% SDS (USB, Cat#75819), 5%  $\beta$ -mercaptoethanol (Sigma, Cat#M7154), Bromophenol blue (Sigma, Cat#B8206), 10% glycerol(USB,Cat#16374) and PVDF- membrane from MilliPore (Cat# IPVH0010).. Tris Buffered Saline (TBS) contains Tris

(50mM) (Affymetrix, #75825), NaCl (150mM) (MP Blomed #194848), pH adjusted to 7.5 with 1M HCl, and used with 0.1% Tween-20 (USB, #20606). PDP ester, PDP acid and DEX-PDP were synthesized by using method reported earlier.<sup>37</sup>

### 2.2 General procedures:

The absorption and emission studies were done by a Perkin-Elmer Lambda 45 UV-Visible spectrophotometer and SPEX Fluorolog HORIBA JOBIN VYON fluorescence spectrophotometer with a double-grating 0.22 m Spex1680 monochromator and a 450W Xe lamp as the excitation source at room temperature. The excitation spectra are collected at 430 nm for camptothecin and 554 nm for doxorubicin and the emission spectra are recorded by exciting at the excitation maxima. The samples were purged with  $\text{N}_2$  gas for at least 15-20 minutes prior to photophysical experiments. The size determination of the drug loaded DEX-PDP was carried out by dynamic light scattering (DLS), using a Nano ZS-90 apparatus utilizing 633 nm red laser (at 90 ° angle) from Malvern instruments. The static light scattering experiment (SLS) was carried out using 3D-DLS spectrometer, from LS instruments, Switzerland. The instrument consist of a He Ne laser having wavelength of 632.8 nm, in autocorrelation mode attached to computer using Lab view interface utilizing toluene as reference. The measurement was performed from 20° to 130° by steps of 5. SLS and DLS studies were done by using 0.2 mg/ml solution of drug loaded vesicular solution which was prepared by dispersing the required amount of lyophilized drug loaded polymer powder in PBS and filtered through 0.45  $\mu\text{M}$  filters. This whole procedure was done under laminar air flow cabinet to avoid the other contamination. The reproducibility of the data was checked for at least three times using independent polymer solutions. Atomic force microscope (AFM) images were recorded using VeecoNanoscope IV instrument. The sample was dropcasted on freshly cleaved mica surface. The imaging was carried out in tapping mode using TAP-190AL-G50 probe from Budget sensors with a nominal spring constant of 48 N/m and resonance frequency of 163.5. FEI, QUANTA 200 3D scanning electron microscope was used for recording FE-SEM image of the sample. For FE SEM analysis, the samples were prepared by drop casting on silicon wafers and coated with gold. TEM images were recorded using a Technai-300 instrument by drop casting the sample on formvar coated copper grid. The fluorescent micrographs were collected using Carl Zeiss Axiovert 200 microscope. LSM710 confocal microscope was used for imaging the cells.

### 2.3 Encapsulation of Doxorubicin.HCl into Dextran nano-vesicles:

Water soluble anticancer drug, Doxorubicin.HCl was loaded into the DEX-PDP nano-vesicles by dialysis method. Briefly, 100 mg of DEX-PDP and 2 mg of DOX.HCl was dissolved in 5 ml of DMSO taken in light protected container. To a stirring solution of above mixture, 5 mL of deionized water was added drop wise. The resulting solution were stirred under dark for 12 hours and then dialysed against deionized water using a dialysis membrane having MWCO 3500 (Spectrapor). The water was exchanged 5 times within 24 hours of time period. The entire procedure of dialysis was done in a dark chamber. The dialysed solution were collected after 24 hours, filtered and then lyophilized.

## 2.4 Determination of Drug Loading Content (DLC) and Drug Loading Efficiency (DLE):

Drug loading content and Drug Loading efficiency were found out by absorption spectroscopy. For this purpose, 3 mg of lyophilized DOX loaded DEX-PDP (polymer) was dissolved in 1 ml of DMSO. 100  $\mu$ l of this solution was diluted to 3 ml and the absorbance at 480 nm was determined using UV-Vis spectrophotometer. The amount of doxorubicin loaded in the vesicle was calculated by using Beers law, where molar extinction coefficient of DOX at 480 nm was kept as 11,500. The following equations were used for finding DLE and DLC<sup>37</sup>.

$$\text{DLE (\%)} = \left\{ \frac{\text{Weight of drug in vesicles}}{\text{Weight of drug in Feed}} \right\} \times 100 \%$$

$$\text{DLC} = \left\{ \frac{\text{Weight of drug in vesicles}}{\text{Weight of Drug loaded vesicles}} \right\}$$

DLE and DLC were calculated as 63 % and 12.6  $\mu$ g/mg of polymer respectively.

## 2.5 Encapsulation of Camptothecin and Doxorubicin.HCl into Dextran nano-vesicles:

Dual drug encapsulation abilities of dextran nano-vesicles were confirmed by loading hydrophobic camptothecin and hydrophilic Doxorubicin.HCl simultaneously. The amount of DOX and CPT required for getting 1: 4 and 4: 1 ratio was determined based on the pre-evaluation of drug loading capacity of dextran nano-vesicles. For obtaining 1: 4 (DOX: CPT) ratio, 2 mg of DOX.HCl, 3.5 mg of CPT and 100 mg of DEX-PDP (polymer) were dissolved in 5 ml of DMSO. Deionized water was added drop wise to above solution with moderate stirring. The content stirred for another 12 hours and transferred into a dialysis bag having MWCO 3,500. The dialysis was continued for 24 hours with five water exchange. The entire procedure was done under dark condition. The dialysed solution was filtered to remove unencapsulated drug content and lyophilized to receive dry powder of dual drug encapsulated system. Drug loading content was determined by using absorption spectroscopy as 28.1  $\mu$ g CPT and 12.0  $\mu$ g DOX per milligram of polymer. Similarly, for attaining 4:1 (DOX: CPT) ratio, 2 mg DOX.HCl and 0.20 mg of CPT were loaded into 100 mg DEX-PDP (polymer) as per the protocol stated above. Final DLC was estimated as 1.72  $\mu$ g CPT and 11.2  $\mu$ g DOX per milligram of polymer.

## 2.6 In-vitro Release of DOX from Dextran nano-vesicles:

The release of DOX from nano-vesicles under physiological condition was determined by dispersing 5 mg of drug loaded DEX-PDP in 3 ml of PBS (Phosphate Buffered Saline). This solution was taken in a dialysis bag and the entire tube was immersed in 100 ml of PBS. The whole solution was incubated at 37 °C. At definite time interval 3 ml of PBS was withdrawn from the dialysate and restore with equal volume of fresh buffer. The samples collected at different time interval were analysed by UV-Visible spectroscopy. The absorbance value at 480 nm was used to determine amount of DOX release from the nano-vesicles. The cumulative release of the drug was calculated by using following equation.

$$\text{Cumulative Drug Release} = \left( \frac{\text{Amount of Drug release at time 't'}}{\text{Total amount of drug in the vesicle taken in dialysis tube}} \right) \times 100.$$

## 2.7 Esterase Assisted Release of DOX from Dextran nano-vesicles:

The effect of esterase enzyme on the release of

doxorubicin from the DEX-PDP nano-vesicles was studied by dialysis method. Briefly, 5 mg of DOX loaded DEX-PDP system were dispersed 3 ml PBS and mixed with 10 U esterase enzyme. This entire solution was taken in a dialysis tube and submerged in 100 ml PBS solution. The whole system was incubated at 37°C under dark condition. At specific time points, 3 ml of dialysate was collected and replaced with fresh buffer solution. The sample collected were analysed by UV visible spectrometer to determine the percentage of DOX release at different time points as described previously. The experiment was also performed by adding esterase enzyme 8<sup>th</sup> and 36<sup>th</sup> hour. In this case, *in-vitro* release was started under normal physiological condition, then after 8<sup>th</sup> hour, or 36<sup>th</sup> hour, solution were recovered from dialysis tube and mixed with 10 U esterase enzyme and continued the release studies. The complete drug elution from the DOX loaded dextran nano-vesicles was also studied by adding excess amount (30 U) esterase enzyme to dialysis bag. The rest of the protocol was maintained same as stated above.

## 2.8 In-vitro Release of DOX and CPT from Dextran nano-vesicles:

The release of DOX and CPT from dual loaded vesicle system (both 1:4 and 4:1) or individual cocktails (both 1:4 and 4:1) was studied by similar method as illustrated for only DOX loaded system. Here in absorbance at 480 nm and 370 nm were noted for DOX and CPT respectively. The concentration of CPT was calculated by using Beers Law, where molar extinction coefficient of camptothecin is kept as 11,250 at 370 nm. The effect of esterase on the release of DOX and CPT from dual loaded system was also studied by adding (10 U) esterase into the solution. The entire procedure was done in a light protected container.

## 2.9 Cell Viability Assay (MTT Assay):

To observe the effect of DOX in  $V_{\text{DOX}}$ , and DOX and CPT in dual loaded  $V_{\text{DOX-CPT}}$ , a cell viability assay was performed using wild type mouse embryonic fibroblasts, MCF7 and DLD1. In case of  $V_{\text{DOX}}$ , the concentration of DOX was maintained as 1  $\mu$ M and 0.5  $\mu$ M for all cell lines used in the assay. While in dual loaded nano-vesicles, DOX concentration was retained as 0.5  $\mu$ M for both combinations. CPT concentration hence varied according to the drug molar ratio required to 2  $\mu$ M (1:4 DOX:CPT) and 0.125  $\mu$ M (4:1 molar ratio DOX:CPT). WT-MEFs ( $1 \times 10^3$  cells/well), Cav1<sup>-/-</sup> MEFs ( $1 \times 10^3$  cells/well), MCF7 ( $2 \times 10^3$  cells/well) and DLD1 ( $2 \times 10^3$  cells/well) were each seeded in a 96 well plate (Corning, USA) in 100  $\mu$ l medium with 10 % FBS (Fetal Bovine Serum) and allowed to adhere for 24 hrs. Medium from cells was aspirated and drug samples at the required concentrations diluted in the same medium were added to the cells. A blank 'medium only' control without cells and an 'untreated cells' control was used in each experiment. All control and treated experiment wells were set in triplicates. Cells were incubated for 24 hrs without a change in media and after 24 hrs, drug containing media was aspirated and freshly prepared MTT in sterile PBS (5 mg/ml) was diluted to 50  $\mu$ g/ml in 100  $\mu$ l media with FBS and added to each well. Cells were then incubated with MTT for 4 hrs at 37 °C in the dark in the CO<sub>2</sub> incubator where the cells were grown. Medium with MTT was then aspirated from wells and the purple formazan crystals formed as a result of reduction of MTT by mitochondrial dehydrogenase enzyme from

cells were dissolved in 100  $\mu$ l of 100% DMSO (added per well). The absorbance from formazan crystals was immediately measured using microplate reader at 570 nm (Tecan Plate Reader) and is representative of number of viable cells per well.

Values from the triplicates for each control and treated set were noted and their means calculated. If all three values were variable the sample was not considered for the study. The mean of the absorbance values for the blank control samples was subtracted from the mean values of the untreated control and treated samples respectively. The values thus obtained for the untreated control samples were equated to 100 % and the relative percentage values for drug treated samples were calculated accordingly. Percentage values thus obtained for treated samples were subtracted from the untreated control (100%) to determine the percentage cell death (relative to control). Results thus obtained from a minimum of 3 to a maximum of 6 experiments were compiled and evaluated statistically using a paired two tail T-Test.

## 2.10 Cellular Uptake of DOX and $V_{\text{RHO}}$ by Confocal Microscopy :

Wild type mouse embryonic fibroblasts (WT MEFs), Cav1<sup>-/-</sup> MEFs, MCF7 and DLD1 were seeded at a density of  $1 \times 10^5$  cells on cover slips coated with fibronectin (2 $\mu$ g/ml) to facilitate their attachment and spreading, in 6 well plates. Cells were incubated overnight and treated with the required concentration of free drug or nano-vesicle encapsulated drug (for a maximum of 4hours) or nano-vesicle encapsulated rhodamine (for 48hours). At this time drug-containing medium was aspirated from each well, cells were washed twice with PBS (1mL per wash) and fixed with 3.5 % paraformaldehyde solution in PBS for 15 min at room temperature. The cells were washed thrice with PBS (1 mL per wash) and stained for 35min with phalloidin conjugated to Alexa 488 (Invitrogen) diluted 1:100 in 5 % BSA solution in PBS. This incubation was done in the dark and the excess dye was washed from the cells with PBS. These cover slips were then incubated with DAPI (0.05 $\mu$ g/ml) for 2 min each to stain the nucleus, and then mounted on slides using Fluoromount-G mounting medium (Southern Biotech). Slides were then dried overnight at room temperature in the dark and then imaged using a LSM710 confocal microscope with the  $\lambda$  405nm (blue channel),  $\lambda$  568 nm (red channel) and  $\lambda$  488nm (green channel) lasers.

Images thus obtained were analysed using the Image J analysis software (NIH). Image of the DAPI stained nucleus in cells (blue channel) was separated from the rest and the threshold plugin used to define the border of the stained nucleus. A mask mapping the edge of thresholded nucleus was created and saved as a region of interest (ROI) in the ROI manager. This ROI was then imported into the image for DOX in the cell (red channel) and used to define the nucleus of the cell in this image. The intensity of fluorescence within this ROI (and hence within the nucleus) in the red channel was now measured using Image J. Recorded integrated density values were then divided by the area of the nucleus (defined by the ROI) to determine the intensity per unit area. Values thus obtained for each nucleus in a sample was used to calculate the mean intensity/area. Results thus obtained from minimum of 14 to maximum of 55 cells in different treatments were compiled and differences statistically evaluated

using a paired two tail T-Test. To determine total fluorescence within the cell, the actin network of the cells was stained with phalloidin and the perimeter of the cell defined as above using the same and the mask and ROI created accordingly. The intensity of fluorescence within this ROI (and hence within the cell) in the red channel was now measured using Image J and quantitated as discussed above.

## 2.11 Western Blotting:

$4 \times 10^5$  cells each of WT-MEFs, Cav1<sup>-/-</sup>-MEFs, DLD1 and MCF7 washed with PBS and then lysed in 100 $\mu$ l of 1X SDS-Sample buffer. Cell- equivalent amounts of lysate were resolved using 12.5% SDS-polyacrylamide gels and transferred to PVDF membrane. Blocking was done using 5% non-fat dry milk in TBS+0.1% Tween 20 (TBS-T). Blots were incubated with anti-caveolin antibody (1:5000) followed by anti-rabbit HRP conjugated antibody (1:5000) and anti-tubulin antibody (1:5000) followed by anti-mouse HRP conjugated antibody (1:5000). Tubulin was used as a loading control. Detection was done using West PICO chemiluminescent substrate (Fisher Scientific, Prod# 34080) on Image Quant- Las 4000 system (GE Healthcare Life sciences).

## 3 Results and Discussion

### 3.1 Synthesis of dextran nano-vesicles and Encapsulation of DOX

Briefly dextran (MW = 6000) was suitably modified with hydrophobic bio-resource 3-pendadecylphenol (PDP) via aliphatic ester linkage to produce DEX-PDP derivative (see Figure 1) following our earlier procedure.<sup>37</sup> The synthetic details are given in the supporting information (see scheme SS-1). PDP unit is a unique structure directing agent for polysaccharides vesicular assemblies (dextran and dextrin in water (or PBS)).<sup>37, 38</sup> These nascent dextran nano-vesicles were characterized by dynamic and static light scattering, AFM and electron microscopic techniques and the details are provided in SF-1 to SF-4.<sup>†</sup> Encapsulation of DOX produced DOX loaded nano-vesicles (in the hydrophilic core) which is named as:  $V_{\text{DOX}}$ .

The dynamic light scattering (DLS) histogram of  $V_{\text{DOX}}$  showed mono-modal distribution with the average diameter of the vesicles as  $170 \pm 10$  nm (see Figure 2a). From this data, the hydrodynamic radius ( $R_h$ ) of the  $V_{\text{DOX}}$  was calculated as  $83 \pm 5$  nm. Static light scattering (SLS) analysis of the  $V_{\text{DOX}}$  (see figure 2b) provided the radius of gyration ( $R_g$ ) from their Guinier plot,  $R_g = 77 \pm 5$  nm. The ratio of  $R_g/R_h$  for the  $V_{\text{DOX}}$  was found to be 1.06, which is in good agreement for vesicular assemblies.<sup>37-40</sup> Electron microscope images of  $V_{\text{DOX}}$  showed uniformly distributed  $170 \pm 5$  nm spherical objects with a definite thin hydrophobic membrane which is a characteristic feature of vesicles (see Figure 2c). HR-TEM image (see figure 2c inset) further evident for the existence of the vesicular assemblies with distinct hydrophobic layer of  $3.0 \pm 1$  nm. Tapping mode AFM images of  $V_{\text{DOX}}$  showed the appearance of donut-shaped objects with high periphery and low centre (See Figure 2d) as characteristics of vesicular assemblies.<sup>40,41</sup> The size of the spherical shape was obtained as  $170 \pm 15$  nm (see figure 2f). The height of these nano-vesicles was obtained as  $13 \pm 2$  nm (see SF-5 and SF-6 for more AFM images).<sup>†</sup>

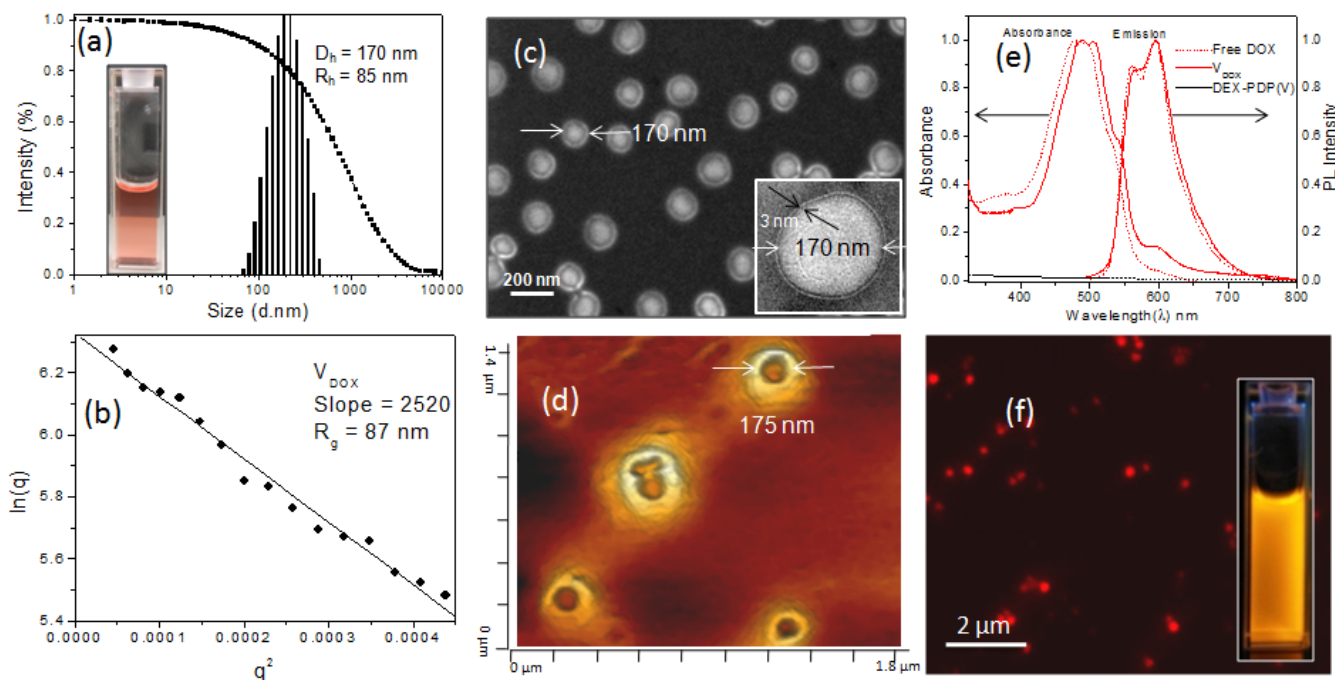


**Fig.2** DLS histogram (a) SLS data (b) FE-SEM image (c) AFM image(d) of  $V_{DOX}$ . Absorbance and Emission plots of free DOX, DOX in Vesicle and Free polymer (e), Fluorescent micrographs of  $V_{DOX}$  (f). The vials insert in (a) and (f) show the color of the vesicles in PBS in visible light and under hand held UV lamp. Insert in (c) shows HR-TEM image of  $V_{DOX}$

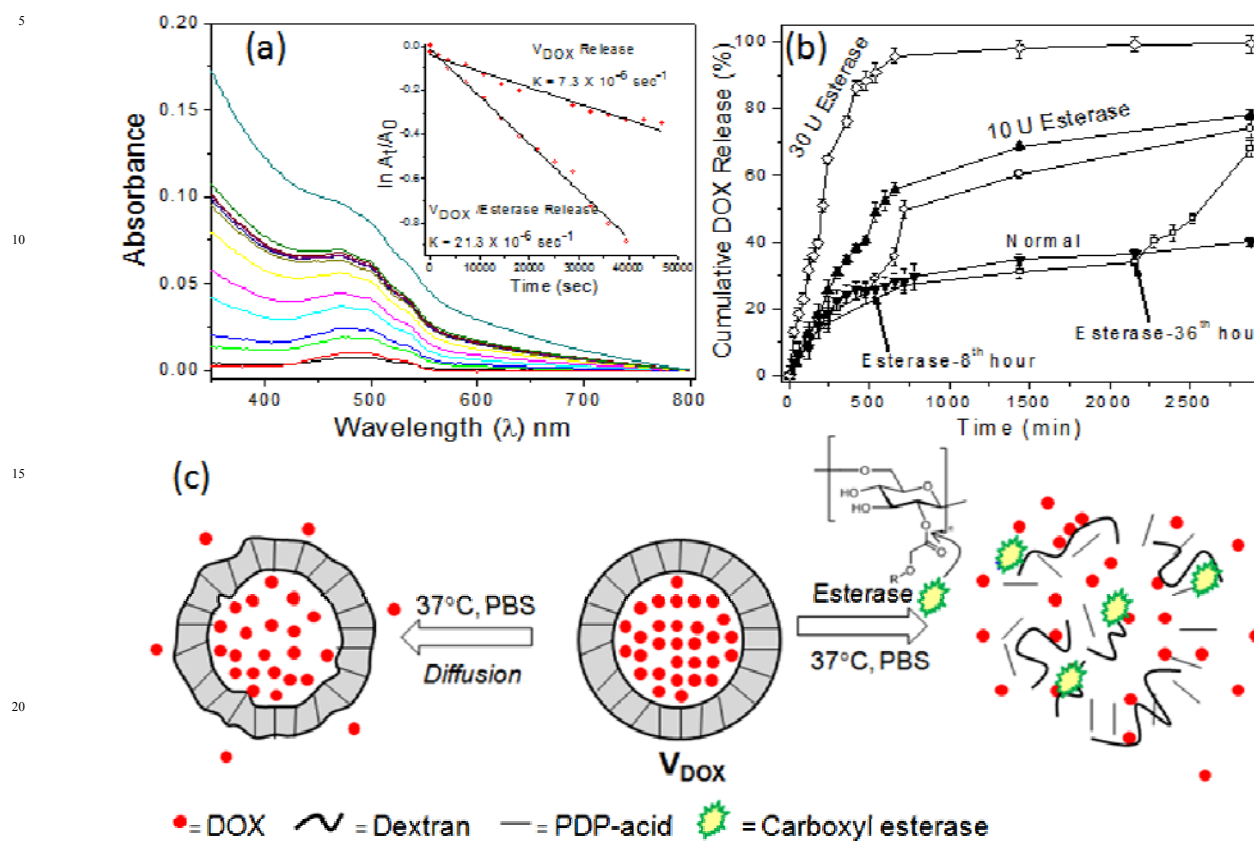
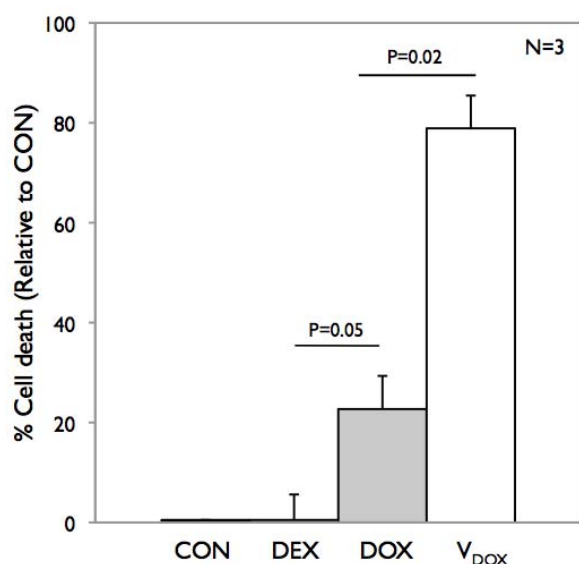


**Fig 3:** (a) Absorbance spectra of DOX release from  $V_{DOX}$ , (b) In-vitro drug release profile of  $V_{DOX}$  in the absence of esterase enzyme, 0 min, 8<sup>th</sup> hour and 36<sup>th</sup> hour of 10U esterase addition and 30 U esterase addition, (c) Mechanism of drug release from vesicle under normal and esterase assisted cleavage. Inset figure in (a) shows  $\ln A_t/A_0$  Vs time plot of  $V_{DOX+CP}$  for the determination of rate constant

DOX is a fluorescent anticancer drug and  $V_{DOX}$  had its absorbance maxima at 480 nm and emission maxima at 590 nm (see figure 2e). The comparison of  $V_{DOX}$  and free DOX indicate that the DOX photophysical characteristics were retained in the dextran nano-vesicle (see figure 2e). Fluorescence microscopic image of  $V_{DOX}$  captured using the RFP filter showed them to be red spherical luminescent objects (see figure 2f). Together this confirms the existence of DOX in the confined vesicular structures. The *in-vitro* release of DOX from  $V_{DOX}$  was studied under physiological conditions to understand the drug release from the core of the vesicles. The drug loaded nano-vesicles were incubated at pH 7.4 at 37 °C in PBS and aliquots were collected at different time interval and analyzed by UV-Visible spectrometer. The absorbance spectra of DOX were used to plot

its release profile from nano-vesicles ( $V_{DOX}$ ) (figure 3a). This showed that about 25 % of drug was discharged in 12 hours and thereafter release occurred in a controlled fashion to release 40 % of the drug in 48 hours (see figure 3b). The capability of esterase enzyme present in cells to cleave the hydrophilic and hydrophobic segments of dextran nano-vesicles was studied *in-vitro* by treating vesicles with 10 U of the enzyme<sup>38</sup> (comparable to amount in some cells). This was seen to promote release of upto 70 % of DOX in 48 hours (Figure 3b). Additionally, if treated with excess of esterase enzyme (30U) 100 % elution of DOX was observed in 10 hours, confirming the susceptibility of these dextran nano-vesicles to cleavage by the esterase enzyme.

(a)



(b)

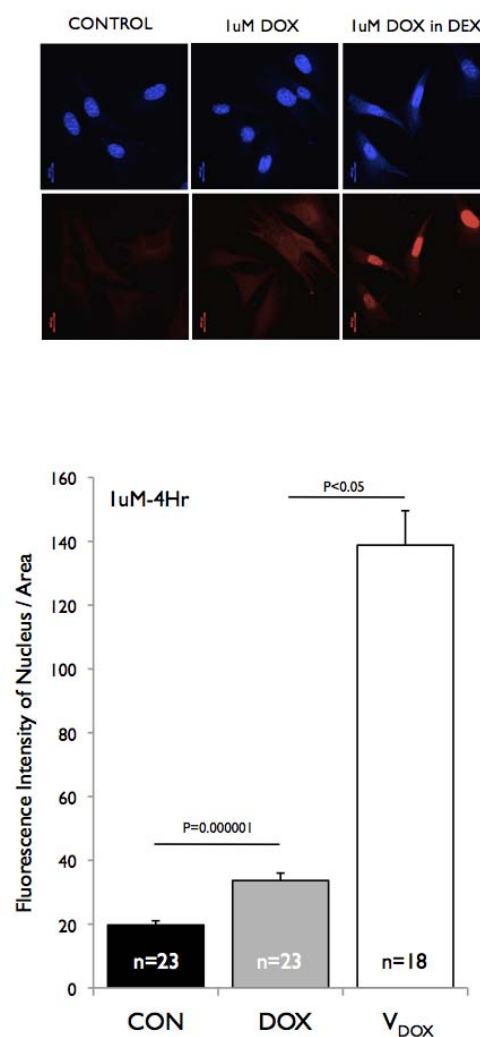


**Fig 4:** (a) Cytotoxicity and uptake of DOX vs  $V_{DOX}$  in WTMEFs. MTT assay was used to test the cytotoxicity of free DOX and  $V_{DOX}$  were compared to DEX-PDP empty vesicle alone and normalized to killing observed in untreated control (CON) at 1µM concentration of drug. Graph represents Mean  $\pm$  SE of percentage cell death relative to control in three independent experiments. (b) Uptake of 1µM DOX and  $V_{DOX}$  was visualized by confocal microscopy in WTMEFs where the nucleus was counter stained with DAPI. Graph represents Mean  $\pm$  SE of DOX fluorescence in the nucleus from indicated number of cells. Data is representative of one in two independent experiments that gave similar results. Statistical analysis was done using standard T Test.

35

Two additional experiments were performed to prove the drug retention capability and slow release capability of DOX containing dextran nano-vesicles. Normal release of DOX from the dextran nano-vesicle was interrupted by addition of esterase enzyme (10U) at 8 hours and 36 hours after vesicles were incubated at physiological conditions (PBS at 37 °C). In both experiments (see figure 3b), an initial 25 to 30 % drug release was followed by an augmented release of the encapsulated DOX content on addition of the esterase enzyme at 8 hrs and 36

10 hrs time points. This suggests the availability of unreleased drug in nano-vesicles for release and action at the target site for upto 36 hrs, till it sees the esterase enzyme. A schematic model for the DOX release from the vesicular structure is shown in figure 3c. In PBS buffer at 37°C, under larger dilution, the nano-vesicles undergo natural leaching out to release about 25 % of the drugs. In the presence of esterase enzyme, the aliphatic ester linkage which connects the dextran to the PDP cleaved instantaneously to releases significant amount of the drugs.

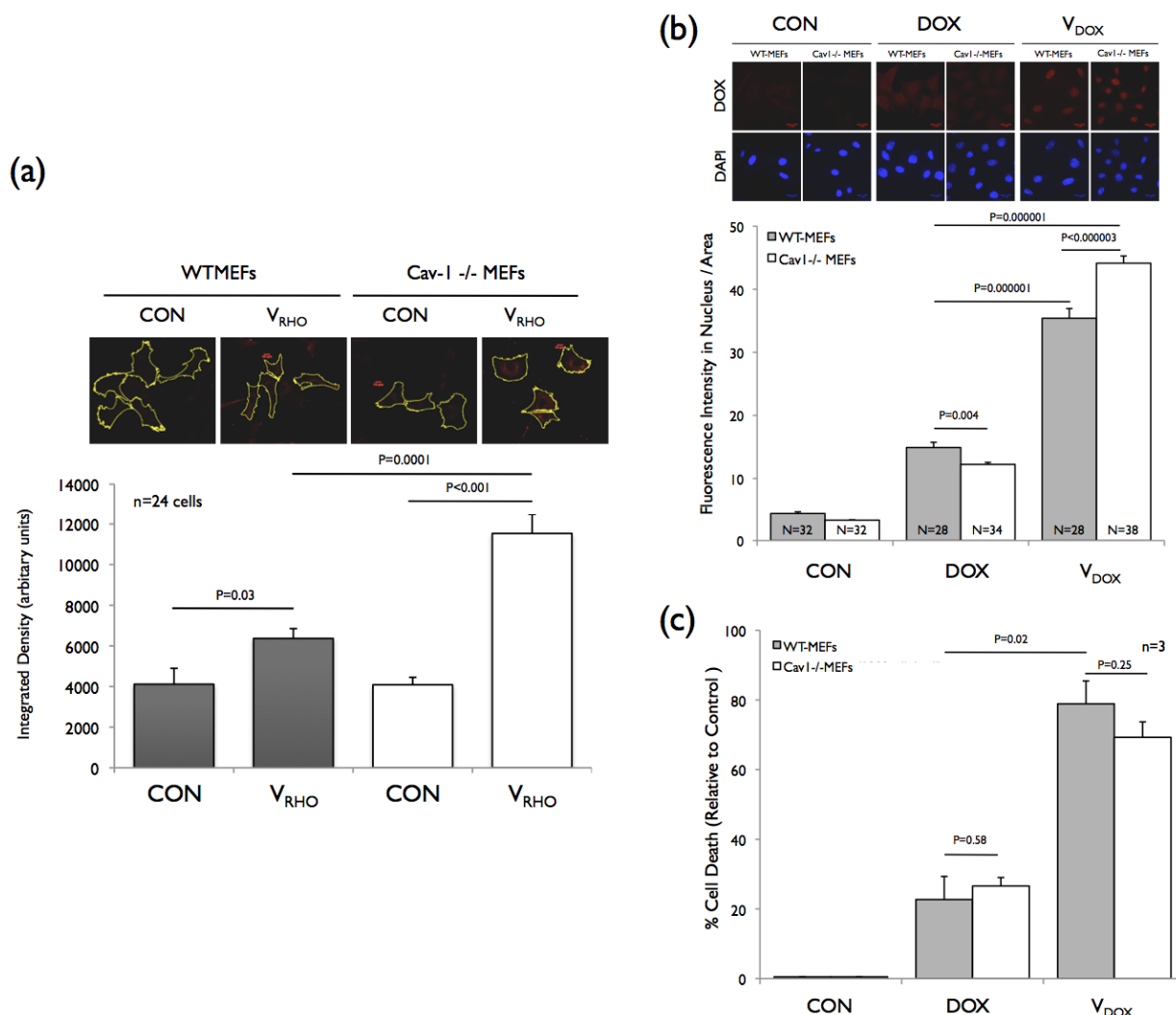


**Fig 5:** Nanovesicle uptake and killing in WT and caveolin-1<sup>-/-</sup> MEFs. (a) Uptake of V<sub>RHO</sub> in WT and Caveolin-1<sup>-/-</sup> MEFs was visualized by confocal microscopy after 48hour treatment. Fluorescence intensity within in the cell perimeter marked by the yellow line was measured and compared between V<sub>RHO</sub> treated and untreated control cells. Graph represents Mean ± SE of rhodamine fluorescence measured as integrated density from indicated number of cells for each treatment. Data is representative of two similar independent experiments that gave similar results. (b) Uptake of 1μM DOX and V<sub>DOX</sub> was visualized by confocal microscopy in WT and caveolin-1<sup>-/-</sup> MEFs where the nucleus was counter stained with DAPI. Graph represents Mean ± SE of DOX fluorescence in the nucleus from indicated number of cells. Data is representative of one in two independent experiments that gave similar results. (c) MTT assay was used to test the cytotoxicity of free DOX and V<sub>DOX</sub> relative to untreated control (CON) at 1μM concentration. Graph represents Mean ± SE of percentage cell death relative to control in three independent experiments and statistically analysed using the standard T Test.

35

30

40

### 3.2 Cytotoxicity and Endocytosis of $V_{DOX}$

The cytotoxic effects of the  $V_{DOX}$  nano-vesicle were first tested on wild type mouse fibroblasts (WTMEFs). The effect of DOX in  $V_{DOX}$  and as free (unloaded) drug was compared at 1.0  $\mu\text{M}$  in these studies. WTMEFs showed  $\approx 20\%$  killing with free DOX while  $V_{DOX}$  killed  $> 2$  fold better (see figure 4a). Empty dextran nano-vesicle (DEX) at concentrations used in the above studies did not significantly affect WT MEFs (figure 4a). Earlier studies on DOX polymer vesicles based on amphiphilic di- and tri-block copolymers,<sup>44-47</sup> poly(g-benzyl L-glutamate)-block hyaluronan,<sup>48</sup> and plasmonic vesicles having gold nanoparticles<sup>49</sup> were found to exhibit better kill cancer cells than DOX alone.<sup>50,51</sup> In our studies this difference is also observed to be more prominently with 2 fold increase in killing of WT MEFs when compared to free DOX (at 1  $\mu\text{M}$ ). One possible explanation for this enhanced killing could be that following the endocytosis of nano-vesicle their directed targeting to specific endocytic compartment and possible simultaneous release of the drug may impact the efficiency and localization of DOX released. This is possibly reflected in better uptake and targeting of DOX in the nucleus as well (Figure 4b). To evaluate this we have looked at the fluorescence of DOX at  $\sim 595\text{nm}$  on binding DNA<sup>52</sup> in treated cells. DOX, a DNA major-groove intercalating agent as well as topoisomerase type-II inhibitor is known to accumulate in the nucleus. The nucleus when mapped in these studies by staining for DAPI shows a close overlap with the DOX fluorescence (SF-7)<sup>†</sup>. DOX fluorescence in the nucleus in  $V_{DOX}$  treated cells was significantly more ( $> 4$  fold) than DOX alone treated cells (figure 4b). Free DOX localization in the nucleus has been ascribed earlier to diffusion<sup>46</sup> while in the case of  $V_{DOX}$  improved uptake into the cell of the drug and / or better targeting to the nucleus

could mediate the DOX accumulation seen. This increase in fluorescence is also seen despite the fact that DOX binding to DNA quenches some of its fluorescence.<sup>49</sup> The increased accumulation of the drug in the nucleus could hence result in better targeting of topoisomerase II in the nucleus supporting a better killing by  $V_{DOX}$  (Figure 4a).

Caveolae are cholesterol and sphingo-lipid rich plasma membrane invaginations formed by the presence of the structural transmembrane protein caveolin (isoforms caveolin-1, -2 and -3).<sup>54,55</sup> Loss of caveolin-1 has been seen to disrupt the formation of caveolae and affect caveolar endocytosis. Fibroblasts from Caveolin-1 knockout mice hence provide a clean system to test the role of caveolae in nano-vesicle endocytosis. Considering that  $V_{DOX}$  uptake is best visible following the nuclear localization of DOX, it may not be an accurate measure of cellular uptake. These studies were hence done using dextran nano-vesicles loaded with the fluorescent water soluble dye Rhodamine B ( $V_{RHO}$ ) (details are given in SF 8)<sup>†</sup>. Litter matched WT (*cav-1<sup>+/+</sup>*) and caveolin-1 lacking (*cav-1<sup>-/-</sup>*) MEFs obtained from the lab of Dr. Richard Anderson<sup>56,57</sup> were compared and their uptake of Rhodamine containing dextran nano-vesicle ( $V_{RHO}$ ) studied over 48hours. Fluorescence intensity measurements for rhodamine at  $\lambda = 596$  nm showed caveolin-1<sup>-/-</sup>MEFs to have  $\sim 2$  fold higher levels of rhodamine fluorescence (reflective possibly of vesicle uptake) than WT MEFs after 48hours (figure 5a). Most of this fluorescence is seen to be in the cytosol, reflecting a better internalization of  $V_{RHO}$  into the cell. This shows caveolar endocytosis to not be a major pathway for uptake of these dextran nano-vesicles ( $V_{RHO}$ ) and also suggests that loss of caveolin-1 (and caveolae) could (directly or indirectly) promote uptake of the dextran nano-vesicles in cells.

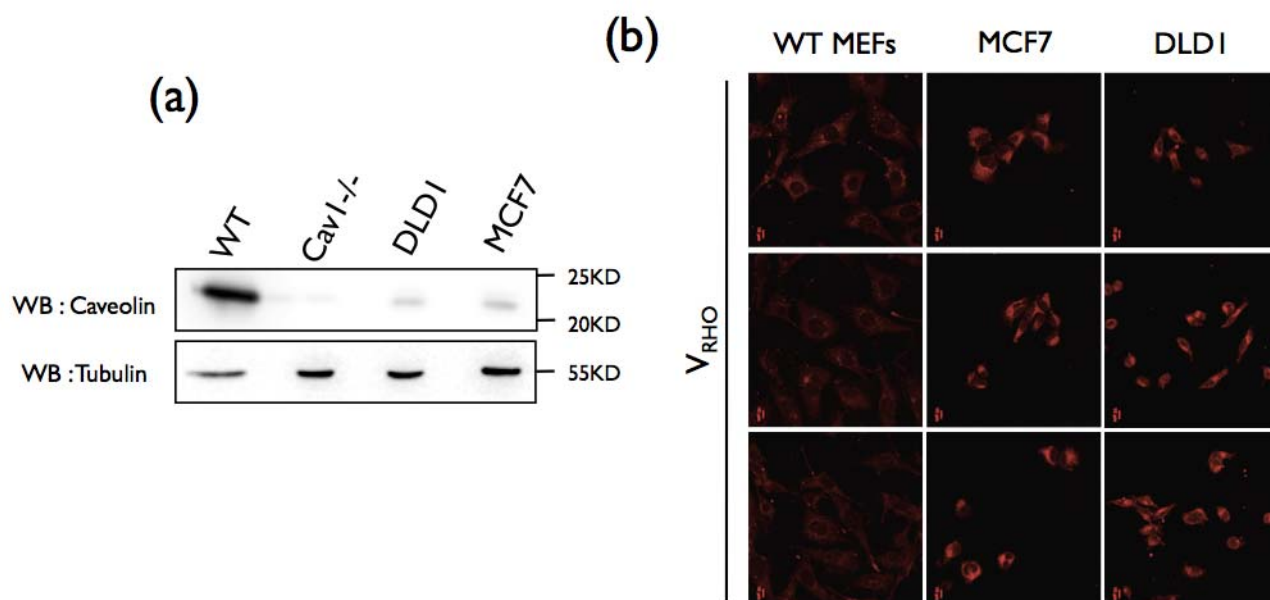
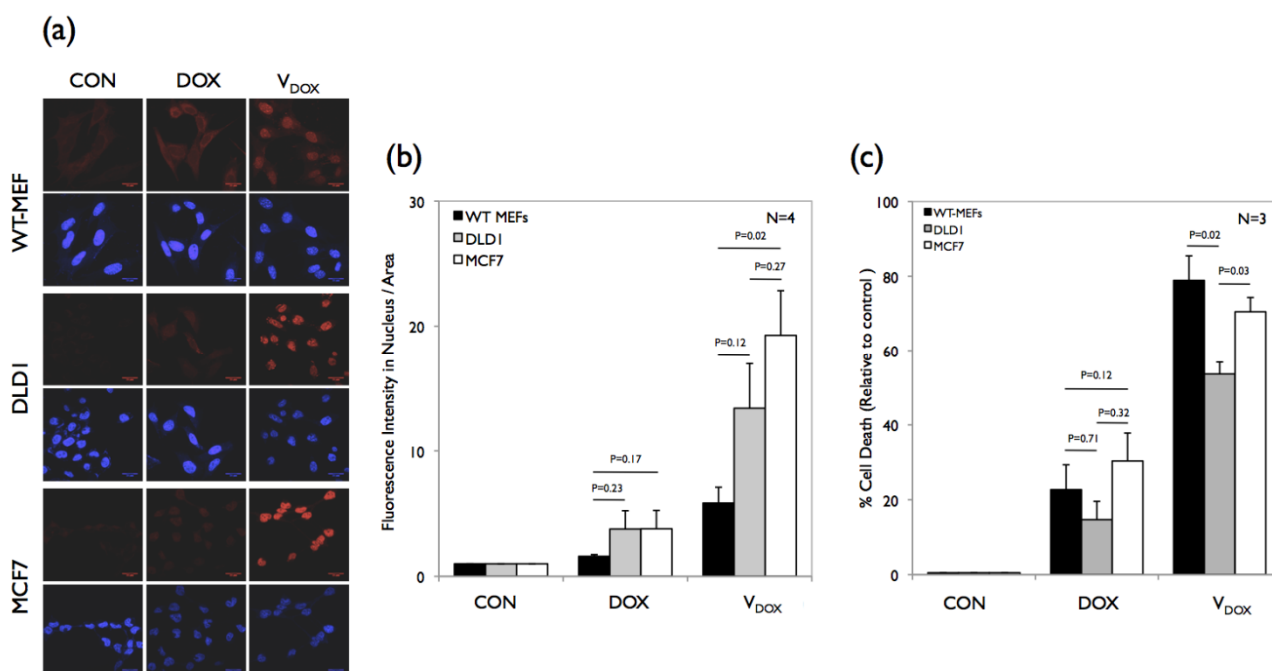


Fig.6 Caveolin-1 expression and uptake of  $V_{RHO}$  in cancer cells. (a) Western Blot detection of Caveolin-1 ( $\sim 22$  KD) in WT MEFs, *cav1*  $-/-$  MEFs, DLD1 and MCF7, relative to the tubulin ( $\sim 55$  KD) loading control. Figure is representative of three independent experiments that gave similar results. (b) Uptake of  $200\mu\text{M}$   $V_{RHO}$  in WTMEFs, MCF7 and DLD1 was visualized by laser confocal microscopy.



**Fig.7**  $V_{DOX}$  uptake and killing in normal vs cancer cells. (a) Uptake of  $1\mu\text{M}$  DOX and  $V_{DOX}$  (red) over 4 hours was visualized by confocal microscopy in WTMEFs, DLD1 and MCF7 cells, where the nucleus was counter stained with DAPI (blue). (b) Graph represents Mean  $\pm$  SE of DOX fluorescence in the nucleus from  $\geq 10$  cells for each treatment in four independent experiments. (c) MTT assay was used to test the cytotoxicity of free DOX and  $V_{DOX}$  relative to untreated control (CON) at  $1\mu\text{M}$  concentration over 24 hours. Graph represents Mean  $\pm$  SE of percentage cell death relative to control in three independent experiments. Statistically analysis for this data was done using the standard T-Test.

Earlier studies characterizing cav-1<sup>-/-</sup> MEFs have reported the plasma membrane order (detected using the membrane intercalating dye laurdan) and possibly cholesterol composition in these cells to be significantly altered as a result of the loss of caveolar endocytosis.<sup>58</sup> This has been seen to regulate among other things cell spreading, migration and growth signaling in the cav-1<sup>-/-</sup> MEFs<sup>52-58, 61</sup>. Loss of caveolin in adipocyte cell line is also seen to promote endocytosis and degradation of insulin receptors.<sup>62</sup> Changes in membrane composition and order could similarly affect nano-vesicle uptake.

To test if the better uptake of  $V_{RHO}$  is reflected in better killing of cav-1<sup>-/-</sup> MEFs cells, the uptake and hence nuclear accumulation of DOX and killing by free DOX vs  $V_{DOX}$  was tested in these cells and compared to WTMEFs. Free DOX showed significantly less nuclear fluorescence in cav-1<sup>-/-</sup> MEFs (Figure 5b) while  $V_{DOX}$  showed significantly more fluorescence in cav-1<sup>-/-</sup> MEFs (Figure 5b) when compared to WTMEFs.

This suggests that the DOX nano-vesicle uptake into the cell and delivery of drug into the nucleus could both be differential in caveolin-1 lacking cells. While  $V_{DOX}$  was seen to kill both cell types better than free DOX, killing of cav-1<sup>-/-</sup> and WT MEFs was not significantly different (Figure 5c). One cause for this could be the differential quenching of DOX following its binding to DNA that contributes to its net fluorescence in the nucleus. This would affect the correlation of nuclear DOX fluorescence with DOX levels in the nucleus and hence cell

killing. This effect might be more prominent for greater DOX uptake levels and smaller differences in DOX nuclear fluorescence observed. In case of larger differences in fluorescence such as between  $V_{DOX}$  and DOX treated cells (in both WTMEFs and Cav-1<sup>-/-</sup> MEFs) quenching may not be a major influencing factor and hence a good correlation does exist between nuclear DOX fluorescence intensity and cell killing (Figure 5c).

To further understand the differential uptake vs killing seen in Cav-1<sup>-/-</sup> MEFs these studies were extended to caveolin-1 lacking cancer cells as well. Caveolin-1 is a known tumor suppressor whose levels are down regulated in many cancers.<sup>26</sup> Two caveolin-1 lacking cancer cell lines identified from literature were studied, MCF7 (breast cancer)<sup>46</sup> and DLD1 (colon cancer).<sup>47</sup> Their caveolin-1 expression when compared to WTMEFs was seen to be less than 10 fold (WTMEF >>>>> MCF7 > DLD1 > Cav-1<sup>-/-</sup>MEFS) (Figure 6a). Like in cav-1<sup>-/-</sup> MEFs (Figure 5a) cytosolic  $V_{RHO}$  fluorescence in MCF7 and DLD1 cells following their incubation with the nano-vesicle is seen to be significantly more than in 'normal' WTMEFs (Figure 6b) suggesting better uptake by the caveolin-1 lacking cancer cells. Nuclear accumulation of free DOX while marginally better in cancer cells was significantly better when administered in  $V_{DOX}$  (Figure 7a). This again was seen to be different between the two cancer cell types, with MCF7 > DLD1 > WTMEFs. This suggests that uptake/nuclear targeting could be influenced by more than just the loss of caveolin-1 levels in these cells.

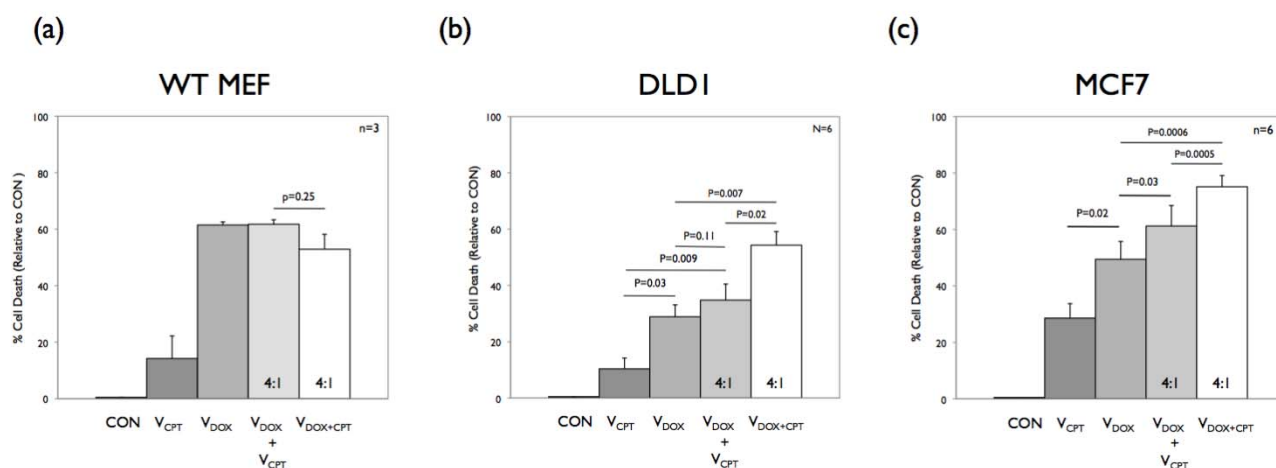


**Fig.8** Killing by DOX:CPT combination at the 4:1 molar ratio.  $V_{DOX}$  ( $0.5\mu M$ ) and  $V_{CPT}$  ( $0.125\mu M$ ) were administered together in separate nano-vesicles ( $V_{DOX+V_{CPT}}$ ) or the same nano-vesicle ( $V_{DOX+CPT}$ ) in WTMEFs (a), DLD1 cells (b) and MCF7 cells (c). Cell killing was analyzed using the MTT assay and percentage cell death relative to untreated control calculated. Graph represents the mean  $\pm$  SE data from three (WTMEF) and six (DLD1, MCF7) independent experiments.

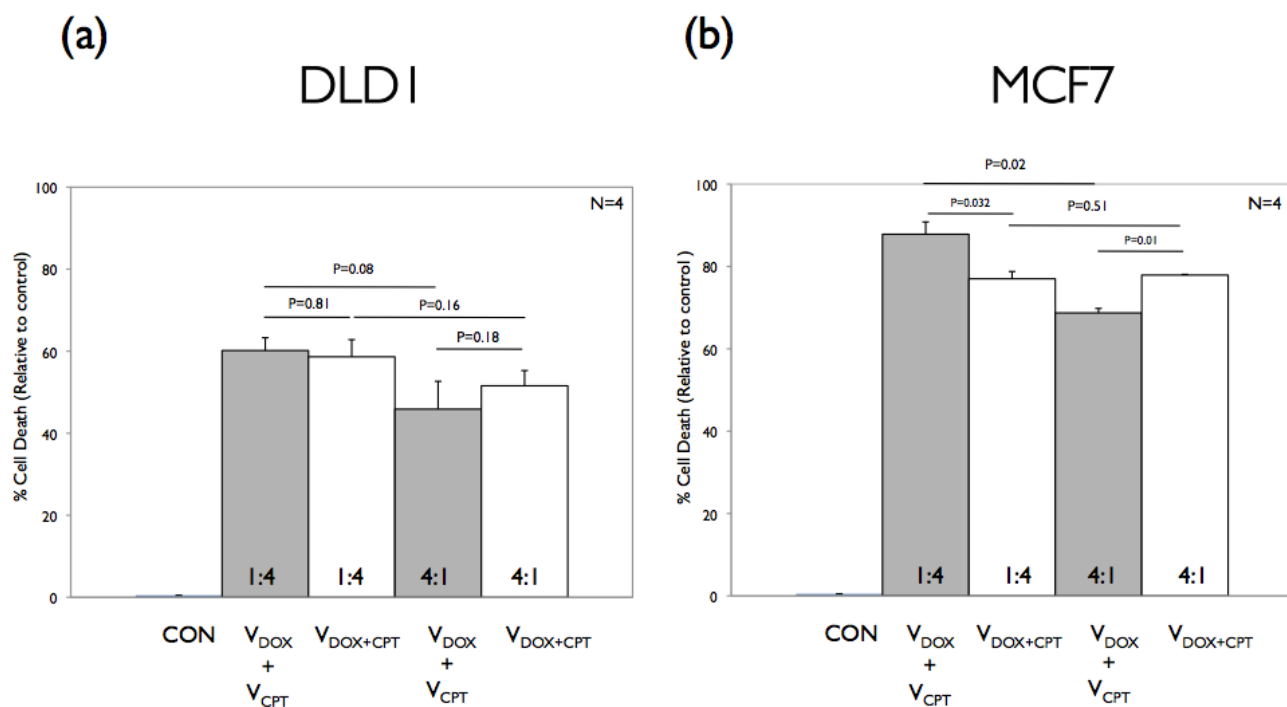
The association between increased nuclear fluorescence and cell killing when tested in these cells (Figure 7b and Figure 7c) showed (a)  $V_{DOX}$  with better nuclear accumulation than free DOX does kills all three cell types better but (b) differences in nuclear accumulation of  $V_{DOX}$  between cell types did not directly correlate with better killing. MCF7 and DLD1 cells with significantly greater nuclear DOX fluorescence in  $V_{DOX}$  treated cells were killed almost as well as WTMEFs. To allow for better visibility and quantitation of differences in the nuclear DOX fluorescence uptake studies are done after a 4 hour treatment with the drug and nano-vesicle. MTT assays were done after a 24 hour treatment with drugs (at the same  $1\mu M$  concentration). The above results could reflect this difference or be a result of the differential quenching of DOX fluorescence in these cell types at different time points making a direct correlation of DOX nuclear fluorescence at 4hours as a measure of its levels in the nucleus difficult, especially across different cell types. Difference in susceptibility to killing by DOX has been reported in cancer cells which could also contribute to this.

### 3.3 Multi Drug Loading and Delivery

One way to improve the killing by DOX in cancer cells is to use it in a ratiometric combination with a drug that could support a synergistic action. Our earlier studies with the water insoluble topoisomerase type I inhibitor CPT have shown the  $V_{CPT}$  nano-vesicle to kill WTMEFs significantly better than free CPT.<sup>37</sup> The improved killing of these WTMEFs by topoisomerase type II inhibitor  $V_{DOX}$  shown in the present studies raises the exciting possibility of creating a combined  $V_{CPT+DOX}$  nano-vesicles for testing in cancer cells. Encapsulation of DOX and CPT produced pink or magenta fluorescent CPT and DOX dual loaded nano-vesicles ( $V_{DOX+CPT}$ ) (see SF-9 for  $V_{CPT}$ ). These nano-vesicles were produced in two different molar ratios of DOX:CPT, 4:1 and 1:4, to study their ratiometric effect.

The dual loaded nano-vesicle ( $V_{DOX+CPT}$ ) was also

found to show mono-model distribution of average sizes of  $220 \pm 15$  nm in the DLS (see SF-10a)<sup>†</sup>. The radius of gyration  $R_g = 113$  nm was obtained from SLS studies and the ratio of  $R_g/R_h = 1.05$  (see SF-10b)<sup>†</sup> confirmed the vesicular assemblies in the dual loaded scaffold  $V_{DOX+CPT}$ .<sup>40</sup> Similarly, Electron microscopic images of the dual loaded nano-vesicle  $V_{DOX+CPT}$  (1:4 and 4:1) was found to be spherical in shape with average size of  $205 \pm 10$  nm (see SF-10c)<sup>†</sup>. The AFM image of  $V_{DOX+CPT}$  (1:4 and 4:1) appeared as donut shaped with inner curvature as typically observed for vesicular assemblies.<sup>41</sup> The size of the vesicular structure was obtained as  $200 \pm 15$  nm (see SF-10d)<sup>†</sup>. The height of these nano-vesicles obtained from the cross sectional analysis as  $10 \pm 3$  nm. The sizes of objects in the images are in very good agreement with the DLS (and also with SLS) data.  $V_{DOX+CPT}$ , showed two absorbance maxima at 370 and 480 nm with respect to the presence of CPT and DOX, respectively (See SF-10e)<sup>†</sup>. Upon photo-excitation at 370 nm, only CPT emission was observed and there is no emission from DOX. The photo-excitation at 480 nm produced exclusively DOX emission at 590 nm in the  $V_{DOX+CPT}$  (see SF-10e)<sup>†</sup>. This suggested that the drug molecules were completely segregated in the nano-vesicle and no FRET was visible between them. Fluorescence microscopic images of  $V_{CPT}$  and  $V_{DOX}$  were observed as blue and red spherical luminescent objects (See Figure 2f and SF-10f)<sup>†</sup>, whereas  $V_{DOX+CPT}$  appeared as pink colored spherical particles. (For details see SF-11)<sup>†</sup>. The absorbance spectra of the release profiles of dual loaded nano-vesicle  $V_{DOX+CPT}$  (1:4) are shown in SF-12a. These show the release of both DOX as well as CPT occurred simultaneously from the dual loaded nano-vesicles, but CPT levels released was much higher than DOX (see SF-12b)<sup>†</sup>. Esterase enzyme mediated release of drugs from the dual loaded nano-vesicles  $V_{DOX+CPT}$  (molar ratio 1:4 and 4:1) and cocktail of individual drug loaded nano-vesicles  $V_{DOX} + V_{CPT}$  (molar ratio 1:4 and 4:1) when compared were similar (see SF-12c to SF-12f) for esterase assisted drug release and for normal release SF-13)<sup>†</sup>.



5

**Fig.9** Killing by DOX:CPT combination at the 1:4 vs 4:1 molar ratio. DOX and CPT were administered together (in separate nano-vesicles –  $V_{DOX}+V_{CPT}$ ) or the same nano-vesicle ( $V_{DOX+CPT}$ ) in DLD1 cells (a) and MCF7 (b) cells at 1:4 (0.5  $\mu$ M: 2  $\mu$ M) molar ratios and 4:1 (0.5  $\mu$ M: 0.125  $\mu$ M). Cell killing was analyzed using the MTT assay and percentage cell death relative to untreated control calculated. Graph represents the mean  $\pm$  SE data from four independent experiments.

10 The release profile of the drugs from dual drug loaded nano-vesicles was followed in a similar manner as of their individual cocktails (see SF-12c to SF-12f for esterase assisted drug release and for normal release SF-13)<sup>†</sup>. Interestingly, both 1:4 and 4:1 molar ratio loaded nano-vesicles exhibited similar 15 drug release pattern. Under normal conditions the release of DOX went upto 35  $\pm$  5 % and that of CPT reached 55  $\pm$  3 % in 48 hours in both type of nano-vesicles. As observed in DOX loaded nano-vesicles, esterase enzyme helped the breakdown of these nano-vesicles causing better release of DOX (65  $\pm$  4 %) and CPT (~100%) in 48 hours. The ratio of the number of moles of DOX released to number of moles of CPT released were determined and plotted against time (see inset in SF-12c to SF-12f)<sup>†</sup> to study the actual ratio of the drug that will reach the target cell. The 4:1 (DOX:CPT) dual drug loaded and individual cocktails of nano-vesicles attained the DOX to CPT discharge ratio as 3:1 in 6 hrs 25 time period and maintained this ratio. But in the case of 1:4 (DOX:CPT) dual drug loaded nano-vesicles, the drug discharge ratio reached 1:4 in 8 hrs (1:4 in 6 hours also) while the individual 1:4 cocktails reached a 1:6 discharge ratio in 6 hrs. 30 This suggest that the layer loaded CPT is released faster than when compared to nano-vesicles where the core is loaded with DOX. Earlier studies have suggested that a combination of topoisomerases I and II inhibitors may be synergistic when administered together.<sup>33</sup> Many cancer cell types seen to be 35 resistant to camptothecin when treated in combination with DOX were seen to be additive or antagonistic depending on their molar ratio.<sup>35,65</sup> Schedule-dependency is also reported with

topoisomerase inhibitors, treatment with topoisomerase 1 inhibitor (such as CPT) followed by a topoisomerase 2 inhibitor (such as DOX) seen to be synergistic.<sup>63,65</sup> Considering the same, the rate constant (k) for the drug release from the nano-vesicles was calculated for CPT and DOX using first order rate equation,<sup>66</sup>  $\ln(A_t/A_0)=-kt$ , where  $A_t$  and  $A_0$  are corresponding to drug in the nano-vesicles at time 't' and initial, respectively (see 45 inset in SF-10a, table –ST-1 and SF-14 for details)<sup>†</sup>. These kinetic parameters revealed that the rate of CPT release from the individual loaded nano-vesicle ( $V_{CPT}$ , 15.3  $\mu$ s<sup>-1</sup>) was two-fold faster than that of DOX from  $V_{DOX}$  (7.3  $\mu$ s<sup>-1</sup>). A similar trend was noted in both the dual loaded nano-vesicles [1:4 and 4:1 DOX:CPT, see table ST-1]. In the presence of esterase enzyme, the release rate of CPT and DOX became three fold faster than their normal release from both individual and dual loaded nano-vesicles. 50

Since molar ratios were reported to be important for 55 this synergistic / antagonistic action between CPT and DOX, we also decided to study and compare the action of the 1:4 DOX:CPT (known to be antagonistic in earlier free drug studies<sup>35</sup>) and 4:1 DOX:CPT molar ratio treatments. These studies were initiated with a 4:1  $V_{DOX+CPT}$  nano-vesicle, testing 60 for its action on WTMEFs vs DLD1 vs MCF7 cells, while comparing it to  $V_{DOX} + V_{CPT}$  (administered at comparable molar concentration but in separate nano-vesicles) and individual drug containing nano-vesicles ( $V_{DOX}$  and  $V_{CPT}$ ).

Results from these studies confirmed  $V_{DOX}$  (at 0.5  $\mu$ M) 65 to kill all three cell types significantly better than  $V_{CPT}$  (at 0.125

$\mu\text{M}$ ) (See Figure 8a). Further, in 'normal' mouse fibroblasts using these drugs in a 4:1 ratio (DOX:CPT) in separate or in the same nano-vesicle did not kill cells significantly better than  $V_{\text{DOX}}$ . This may in part have to do with the fact that in 'normal' fibroblasts  $V_{\text{DOX}}$  by itself kills cells well. In both cancer cells  $V_{\text{DOX}}$  mediated killing is significantly less than that seen in normal cells (See Figure 8b and 8c). Interestingly administering a DOX:CPT drug combination in a 4:1 ratio in these cancer cells killed them significantly better than  $V_{\text{DOX}}$ . Having this drug combination in the same nano-vesicle was also seen to kill cells significantly better than if they were in separate nano-vesicles. Earlier *in-vitro* release studies under physiological conditions have shown the DOX:CPT 4:1 drug nano-vesicle to achieve a final ratio of 3:1 in 6 hours, irrespective of if they are in same or separate nano-vesicles (See SF-12)<sup>†</sup>. This suggests that it is unlikely that major differences in release rates and hence final concentrations achieved may be causing the differential killing observed. This leaves us to speculate that the release of both drugs in close proximity (achieved better with the combined nano-vesicle) might (at this ratio) be important for their improved action in the combined nano-vesicle.  $V_{\text{DOX+CPT}}$  nano-vesicles were thus able to achieve ~80% killing in MCF7 cells and ~60% killing in DLD1 cells.

To further establish that the ratio of the drugs (DOX:CPT) is vital to the enhanced killing observed in cancer cells, we also decided to compare drugs at molar ratio of 4:1 to 1:4 in separate and same nano-vesicle. Contrary to published reports<sup>35</sup> the 1:4 DOX:CPT ratio was not seen to be antagonistic in these studies, killing MCF7 and DLD1 as well or better than 4:1. (Figure 9a, b). Interestingly if administered together in one nano-vesicle, both 1:4 and 4:1 showed almost comparable killing. However, when administered in separate nano-vesicles the 1:4 ratio killed both MCF7 and DLD1 cells better than 4:1 (See Figure 9 a, b). Molar DOX concentrations at both these ratios (1:4 and 4:1) are similar (0.5 $\mu\text{M}$ ) while molar CPT concentration increased from 0.125 $\mu\text{M}$  (in 4:1) to 2 $\mu\text{M}$  (in 1:4). This suggests that having more CPT in the DOX:CPT combination could promote their joint action. This coupled with the two fold faster release of CPT from individual nano-vesicle ( $V_{\text{CPT}}$ ) than the combined ( $V_{\text{DOX+CPT}}$ ) nano-vesicle causes the 1:4  $V_{\text{DOX}} + V_{\text{CPT}}$  treatment to achieve the best killing among all the four combinations tested in both cancer cell lines.

This study provides an insight into the polysaccharide nano-vesicle as multidrug carrier for synergistic killing of cancer cells also highlighting the role ratiometric drug composition could have in the effectiveness of this treatment. Though, this study focuses on only two topoisomerase targeting drugs (DOX and CPT); in principle, the polymer vesicle approach could be applicable to wide range of hydrophobic and hydrophilic drugs which are commercially available. Our ongoing work focuses on expanding these studies to other possible drug combinations as well.

#### 4. Conclusions

In summary, the present work demonstrates the ability to utilize polymer vesicular nano-scaffolds for loading and delivering a topoisomerase I and topoisomerase II targeting drug combination against breast and colon cancer cells. Polysaccharide

nano-vesicles custom designed using renewable resource pendent unit was employed as this multidrug carrier. These dextran nano-vesicles were seen to be capable of loading both hydrophilic DOX and hydrophobic CPT in the core and layer, respectively. These vesicular scaffolds were capable of preserving the anticancer drugs (DOX AND CPT) and release in the presence of the esterase enzyme under physiological conditions. Though vesicular scaffold endocytosis can be mediated by caveolae, endocytosis of this nano-vesicle in caveolae lacking (Cav-1<sup>-/-</sup>) MEFs was seen to be better. This differential uptake is also seen in caveolin-1 (and hence caveolae lacking) breast cancer (MCF7) and colon cancer (DLD1) cells. This is further seen to affect the uptake and nuclear localization of DOX released from  $V_{\text{DOX}}$  in caveolin-1 lacking MCF7 and DLD1 cells supporting their killing. The dual loaded polysaccharide nano-vesicles containing DOX and CPT act synergistically to promote killing of normal MEFs and cancer cells. These studies also revealed the relative ratio of DOX: CPT does affect the differential killing of cancer cells, though the 1:4 ratio reported to be antagonist in earlier studies<sup>35</sup> did not show a similar effect here. When administered as a cocktail having more CPT than DOX (1:4 ratio) synergistic killing of cancer cells was enhanced the most suggesting that a cocktail of these drugs could potentially be the best candidate for delivering multiple anticancer drugs with the best efficacy.

#### Notes and references

<sup>a</sup>Department of Chemistry, <sup>b</sup>Department of Biology  
Indian Institute of Science Education and Research (IISER)-Pune  
Dr. Homi Bhabha Road, Pune – 411008, Maharashtra, India

#### AUTHOR INFORMATION

**Corresponding Author:** Dr. Manickam Jayakannan (e-mail: [jayakannan@iiserpune.ac.in](mailto:jayakannan@iiserpune.ac.in)) and Dr. Nagaraj Balasubramanian ([nagaraj@iiserpune.ac.in](mailto:nagaraj@iiserpune.ac.in))

#### Author Contributions

The manuscript was written through contributions of all authors. All authors have given approval to the final version of the manuscript. #Prمود and Ruchira contributed equally.

#### Acknowledgements

The authors thank research grant from Department of Science and Technology (DST), New Delhi, INDIA, under nanomission initiative project SR/NM/NS-42/2009 and SERB project SB/S1/OC-37/2013. NB was supported by the Ramalingaswami fellowship from the Department of Biotechnology. NB lab is now supported by a Senior Fellowship grant from the Wellcome Trust DBT Alliance. P.S. Prمود thanks IISER Pune for research fellowship. The authors thank National Chemical laboratory, Pune, India for HR-TEM and SLS facilities.

<sup>†</sup> Electronic Supplementary Information (ESI) available: Synthetic Scheme, DLS histogram, FE-SEM Image, AFM image, TEM image of DEX-PDP-5, AFM image of  $V_{\text{DOX+CPT}}$ , AFM image of  $V_{\text{DOX}}$ , Characterization of  $V_{\text{CPT}}$ , Characterization of  $V_{\text{RHO}}$ , DOX Nuclear localization, Characterization of dual drug loaded vesicles, Fluorescent Microscopic image of  $V_{\text{DOX+CPT}}$ , Cumulative drug release profile from dual drug loaded vesicles, Rate constant determination, Cumulative release profile of DOX and CPT from  $V_{\text{DOX+CPT}}$ (1:4), are provided as Supporting Information. See DOI: 10.1039/b000000x/

1. S.-M. Lee, T. V. O'Halloran and S. T. Nguyen, *J. Am. Chem. Soc.*, 2010, 132, 17130-17138.
2. W. Chen, F. Meng, R. Cheng and Z. Zhong, *J. Control. Rel.*, 2010, 142, 40-46.

3. C. Lei, Y. Cui, L. Zheng, P. Kah-Hoe Chow and C.-H. Wang, *Biomaterials*, 2013, **34**, 7483-7494.
4. Y. Xiao, R. Jaskula-Sztul, A. Javadi, W. Xu, J. Eide, A. Dammalapati, M. Kunnimalaiyaan, H. Chen and S. Gong, *Nanoscale*, 2012, **4**, 7185-7193.
5. J. Du and R. K. O'Reilly, *Soft Matter*, 2009, **5**, 3544-3561.
6. P. Tanner, P. Baumann, R. Enea, O. Onaca, C. Palivan and W. Meier, *Acc. Chem. Res.*, 2011, **44**, 1039-1049.
7. F. Meng, Z. Zhong and J. Feijen, *Biomacromolecules*, 2009, **10**, 197-209.
8. O. Onaca, R. Enea, D. W. Hughes and W. Meier, *Macromol. Biosci.*, 2009, **9**, 129-139.
9. S. S. Dhule, P. Penformis, J. He, M. R. Harris, T. Terry, V. John and R. Pochampally, *Mol. Pharm.*, 2013, **11**, 417-427.
10. F. Meng and Z. Zhong, *J. Phys. Chem. Lett.*, 2011, **2**, 1533-1539.
11. B. Surnar and M. Jayakannan, *Biomacromolecules*, 2013, **14**, 4377-4387.
12. B. M. Discher, Y.-Y. Won, D. S. Ege, J. C.-M. Lee, F. S. Bates, D. E. Discher and D. A. Hammer, *Science*, 1999, **284**, 1143-1146.
13. J. Wu and A. Eisenberg, *J. Am. Chem. Soc.*, 2006, **128**, 2880-2884.
14. C. Yuan, K. Raghupathi, B. C. Popere, J. Ventura, L. Dai and S. Thayumanavan, *Chem. Sci.*, 2014, **5**, 229-234.
15. F. Meng, C. Hiemstra, G. H. M. Engbers and J. Feijen, *Macromolecules*, 2003, **36**, 3004-3006.
16. H. J. Lee, S. R. Yang, E. J. An and J.-D. Kim, *Macromolecules*, 2006, **39**, 4938-4940.
17. S. Mizrahy and D. Peer, *Chemical Society Reviews*, 2012, **41**, 2623-2640.
18. W. Wang, A. M. McConaghy, L. Tetley and I. F. Uchegbu, *Langmuir*, 2001, **17**, 631-636.
19. K. K. Upadhyay, J. F. L. Meins, A. Misra, P. Voisin, V. Bouchaud, E. Ibarboure, C. Schatz and S. Lecommandoux, *Biomacromolecules*, 2009, **10**, 2802-2808.
20. E. Blasco, J. L. Serrano, M. Piñol and L. Oriol, *Macromolecules*, 2013, **46**, 5951-5960.
21. J. Wu, H. Tang and P. Wu, *Soft Matter*, 2011, **7**, 4166-4169.
22. Y. Liu, C. Yu, H. Jin, B. Jiang, X. Zhu, Y. Zhou, Z. Lu and D. Yan, *J. Am. Chem. Soc.*, 2013, **135**, 4765-4770.
23. Y. Zhou and D. Yan, *Ang. Chem. Int. Ed.*, 2004, **43**, 4896-4899.
24. W. Tao, Y. Liu, B. Jiang, S. Yu, W. Huang, Y. Zhou and D. Yan, *J. Am. Chem. Soc.*, 2011, **134**, 762-764.
25. F. Ahmed, R. I. Pakunlu, A. Brannan, F. Bates, T. Minko and D. E. Discher, *J. Control. Rel.*, 2006, **116**, 150-158.
26. S. Aryal, C.-M. J. Hu and L. Zhang, *Mol. Pharm.*, 2011, **8**, 1401-1407.
27. T. Thambi, V. G. Deepagan, H. Ko, D. S. Lee and J. H. Park, *J. Mat. Chem.*, 2012, **22**, 22028-22036.
28. A. Feng and J. Yuan, *Macromol. Rapid Commun.*, 2014, n/a-n/a.
29. H. Cai and P. Yao, *Nanoscale*, 2013, **5**, 2892-2900.
30. G. Sahay, D. Y. Alakhova and A. V. Kabanov, *J. Control. Rel.*, 2010, **145**, 182-195.
31. L. M. Bareford and P. W. Swaan, *Adv. Drug Deliv. Rev.*, 2007, **59**, 748-758.
32. T. M. Williams and M. P. Lisanti, *Am. J. Physiol. Cell Physiol.*, 2005, **288**, C494-C506.
33. J. J. Hwang, J. L. Marshall and N. Rizvi, *Oncology (Williston Park, N.Y.)*, 2003, **17**, 46-51.
34. D. C. Marchion, E. Bicaku, A. I. Daud, D. M. Sullivan and P. N. Munster, *Mol. Cancer Ther.*, 2005, **4**, 1993-2000.
35. V. Pavillard, D. Kherfella, S. Richard, J. Robert and D. Montaudon, *Br. J. Cancer*, 2001, **85**, 1077-1083.
36. A. R. Maity, A. Chakraborty, A. Mondal and N. R. Jana, *Nanoscale*, 2014, **6**, 2752-2758.
37. P. S. Pramod, K. Takamura, S. Chaphekar, N. Balasubramanian and M. Jayakannan, *Biomacromolecules*, 2012, **13**, 3627-3640.
38. U. Sridhar, P. S. Pramod and M. Jayakannan, *RSC Advances*, 2013, **3**, 21237-21241.
39. A. R. Maity, A. Chakraborty, A. Mondal and N. R. Jana, *Nanoscale*, 2014, **6**, 2752-2758.
40. C. Houga, J. Giermanska, S. Lecommandoux, R. Borsali, D. Taton, Y. Gnanou and J.-F. Le Meins, *Biomacromolecules*, 2008, **10**, 32-40.
41. M. Yang, W. Wang, F. Yuan, X. Zhang, J. Li, F. Liang, B. He, B. Minch and G. Wegner, *J. Am. Chem. Soc.*, 2005, **127**, 15107-15111.
42. H. Iatrou, H. Frielinghaus, S. Hanski, N. Ferderigos, J. Ruokolainen, O. Ikkala, D. Richter, J. Mays and N. Hadjichristidis, *Biomacromolecules*, 2007, **8**, 2173-2181.
43. G. Xu, W. Zhang, M. K. Ma and H. L. McLeod, *Clinical Cancer Research*, 2002, **8**, 2605-2611.
44. X. Yang, J. J. Grailer, I. J. Rowland, A. Javadi, S. A. Hurley, V. Z. Matson, D. A. Steeber and S. Gong, *ACS Nano*, 2010, **4**, 6805-6817.
45. K.-I. Joo, L. Xiao, S. Liu, Y. Liu, C.-L. Lee, P. S. Conti, M. K. Wong, Z. Li and P. Wang, *Biomaterials*, 2013, **34**, 3098-3109.
46. Y. Du, W. Chen, M. Zheng, F. Meng and Z. Zhong, *Biomaterials*, 2012, **33**, 7291-7299.
47. X. Yang, J. J. Grailer, I. J. Rowland, A. Javadi, S. A. Hurley, D. A. Steeber and S. Gong, *Biomaterials*, 2010, **31**, 9065-9073.
48. K. K. Upadhyay, A. N. Bhatt, A. K. Mishra, B. S. Dwarakanath, S. Jain, C. Schatz, J.-F. Le Meins, A. Farooque, G. Chandraiah, A. K. Jain, A. Misra and S. Lecommandoux, *Biomaterials*, 2010, **31**, 2882-2892.
49. J. Song, J. Zhou and H. Duan, *J. Am. Chem. Soc.*, 2012, **134**, 13458-13469.
50. Y. Ma, Z. Dai, Z. Zha, Y. Gao and X. Yue, *Biomaterials*, 2011, **32**, 9300-9307.
51. R. Jin, X. Ji, Y. Yang, H. Wang and A. Cao, *ACS Appl. Mater. Interfaces*, 2013, **5**, 7181-7189.
52. P. Mohan and N. Rapoport, *Mol. Pharm.*, 2010, **7**, 1959-1973.
53. X. Dai, Z. Yue, M. E. Eccleston, J. Swartling, N. K. H. Slater and C. F. Kaminski, *Nanomed. Nanotech. Biol. Med.*, 2008, **4**, 49-56.
54. L. A. Carver and J. E. Schnitzer, *Nat. Rev. Cancer*, 2003, **3**, 571-581.
55. R. G. Parton and M. A. del Pozo, *Nat. Rev. Mol. Cell Biol.*, 2013, **14**, 98-112.
56. N. Balasubramanian, D. W. Scott, J. D. Castle, J. E. Casanova and M. A. Schwartz, *Nat. Cell Biol.*, 2007, **9**, 1381-1391.
57. M. A. del Pozo, N. Balasubramanian, N. B. Alderson, W. B. Kiosses, A. Grande-Garcia, R. G. W. Anderson and M. A. Schwartz, *Nat. Cell Biol.*, 2005, **7**, 901-908.
58. K. Gaus, S. Le Lay, N. Balasubramanian and M. A. Schwartz, *J. Cell Biol.*, 2006, **174**, 725-734.
59. N. Balasubramanian, J. A. Meier, D. W. Scott, A. Norambuena, M. A. White and M. A. Schwartz, *Current biology : CB*, 2010, **20**, 75-79.
60. N. Patani, L.-A. Martin, J. Reis-Filho and M. Dowsett, *Breast Cancer Res. Treat.*, 2012, **131**, 1-15.
61. F. C. Bender, M. A. Reymond, C. Bron and A. F. G. Quest, *Cancer Res.*, 2000, **60**, 5870-5878.
62. K. Otsu, Y. Toya, J. Oshikawa, R. Kurotani, T. Yazawa, M. Sato, U. Yokoyama, S. Umemura, S. Minamisawa, S. Okumura and Y. Ishikawa, *Am. J. Physiol.-Cell Ph.*, 2010, **298**, C450-C456.
63. S. H. Kaufmann, *Cancer Res.*, 1991, **51**, 1129-1136.
64. N. S. Masumoto N, Esaki T, Tatsumoto T, Fujishima H, Baba E, Nakamura M, Niho Y., *Anticancer Res.*, 1995, **15**, 405-409.
65. J. A. Bonner and T. F. Kozelsky, *Cancer Chemother. Pharmacol.*, 1996, **39**, 109-112.
66. J. Xu, Q. Fu, J. M. Ren, G. Bryant and G. G. Qiao, *Chem. Comm.*, 2013, **49**, 33-35.